INTERNATIONAL BIOMECHANICS
2019, VOL. 6, NO. 1, 75–84
https://doi.org/10.1080/23335432.2019.1642142

Taylor & Francis
Taylor & Francis Group

Metatarsal arch deformation and forefoot kinematics during gait in asymptomatic subjects

Céline Mahieu[a], Patrick Salvia[a,b], Benoît Beyer[c], Marcel Rooze[a,c], Véronique Feipel[a,c] and Serge Van Sint Jan[a]

[a]Laboratory of Anatomy, Biomechanics and Organogenesis, Faculty of Medicine, Université Libre de Bruxelles, Brussels, Belgium; [b]Center for Functional Evaluation, Université Libre de Bruxelles, Brussels, Belgium; [c]Laboratory of Functional Anatomy, Faculty of Motor Sciences, Université Libre de Bruxelles, Brussels, Belgium

ABSTRACT

This study aimed to investigate both foot arch-shaped architecture and forefoot kinematics during gait. Using a dedicated three-compartment forefoot subdivision, we studied asymptomatic subjects and quantified disorders related to the metatarsal arch. Foot motion and arch shape were measured in 30 healthy subjects with a motion-capture system and force plates. Kinematic results were expressed using a novel model, which anatomically divides the forefoot into three parts. This model integrated the medial longitudinal arch angle and the metatarsal arch height and width. During the first part of stance phase, the medial longitudinal arch flattens and all foot segments move toward dorsiflexion. During terminal stance and preswing phase, medial longitudinal and metatarsal arch restoration was noted with plantarflexion of all segments, an eversion and abduction of the medial forefoot, and an inversion and adduction of the lateral forefoot. Kinematics obtained with the proposed forefoot model corroborates metatarsal arch restoration in late stance. This observation supports the fact that foot architecture is supple until midstance and subsequently creates a rigid lever arm with restored arches to support propulsion. This study's results and methods highlight the potential of the three-compartment model for use in clinical decision-making.

ARTICLE HISTORY
Received 29 December 2018
Accepted 23 June 2019

KEYWORDS
Forefoot kinematics; multisegment foot model; foot deformation; medial longitudinal arch; metatarsal arch; gait analysis

1 Introduction

The human foot is a multi-joint mechanism involved in energy absorption during the loading phase of gait and energy restitution during the propulsive phase. In abnormal gait patterns, the non-physiological muscle and joint stresses increase energy expenditure and may result in pathologies. In motion analysis, the foot could be modelled in two ways, i.e. either as a set of rigid bodies that move relative to each other or as a three-dimensional (3D) deformable shape constituted of a set of arches.

Shank, hindfoot, and midfoot motions are commonly described in the literature. Albeit exposed to extremely high mechanical stresses, such as weight, acceleration, and twisting (Bojsen-Møoller 1979), the forefoot remains poorly investigated. Most of the clinical and biomechanical gait models consider the forefoot as a whole (Carson et al. 2001; Stebbins et al. 2006; Leardini et al. 2007). However, several authors (MacWilliams et al. 2003; Tome et al. 2006; Jenkyn and Nicol 2007; Okita et al. 2009; Rouhani et al. 2011;) demonstrated clinical limitations related to such conception and investigated forefoot kinematics using two-compartment models. Tome (Tome et al. 2006) subdivided the forefoot into metatarsal I and metatarsals II, III, IV, V; Jenkyn (Jenkyn and Nicol 2007) into metatarsals I, II and metatarsals III, IV, V; Mac Williams (MacWilliams et al. 2003) and Rouhani (Rouhani et al. 2011) into metatarsals I, II, III and metatarsals IV, V. Moreover, few studies have integrated a three-compartment forefoot model for studying plantar pressure (Grampp et al. 2000; Queen et al. 2010; van der Zwaard et al. 2014) or Lisfranc joint complex (i.e. tarsometatarsal articulations) after traumatic injury (Komenda et al. 1996). This three-compartment subdivision considers both anatomical (Castro et al. 2010) and various functional aspects (De Doncker and Kowalski 1979; MacWilliams et al. 2003; Nester et al. 2007; Rouhani et al. 2011) of Lisfranc joint complex (Figure 1). While these studies focused on plantar pressures and clinical evaluation in pathological conditions, kinematics of such forefoot division has yet to be investigated.

The 3D shape of the foot has been previously described as a tripod with three supporting points (i.e. anteriorly, the metatarsal heads I and V; posteriorly, the posterior tuberosity of the calcaneus) connected by three

CONTACT Céline Mahieu cmahieu@ulb.ac.be Laboratory of Anatomy, Biomechanics and Organogenesis (LABO), Faculty of Medicine, Université Libre de Bruxelles (CP 619), Route de Lennik, 808, B-1070 Bruxelles, Brussels, Belgium

arches (i.e. medial and lateral longitudinal arches and metatarsal arch) (Kapandji 2011). Such arch-shaped architecture, including bones and soft tissues, plays a significant role in energy absorption and restitution (MacWilliams et al. 2003). While a commonly accepted relationship between the medial longitudinal arch and foot kinematics has been established (Simon et al. 2006; Leardini et al. 2007), the metatarsal arch function remains controversial. Pedobarometric studies did not support the idea of a functional metatarsal arch (Luger et al. 1999; Kanatli et al. 2003; Daentzer et al. 2003) given that the highest pressures are recorded under the second and third metatarsal heads rather than at the supporting points. Nonetheless, recent studies demonstrated the existence of metatarsal osseous arch (Simonsen et al. 2009) and its restoration during late stance (Duerinck et al. 2014). Of note, these results were not observed by means of a multisegment foot model.

Changes in kinematics and forefoot shape could be related to clinical impairments. For example, a flattened metatarsal arch is believed to be the most common cause of metatarsalgia and is frequently associated with foot deformities (e.g. splayfoot, hallux valgus, and claw toes) (Tschauner and Kohlmaier 1997; Simonsen et al. 2009). Hence, a more accurate foot assessment that focuses on forefoot motion patterns in relation to forefoot shape is needed, and the assessment data could also provide relevant information for modeling purposes and for designing orthotic insoles.

Thus, this study aimed to investigate both arch-shaped architecture and forefoot kinematics during gait in a sample of asymptomatic subjects. The novel foot model using an especially dedicated three-compartment forefoot subdivision will enable the quantification of the metatarsal arch deformation.

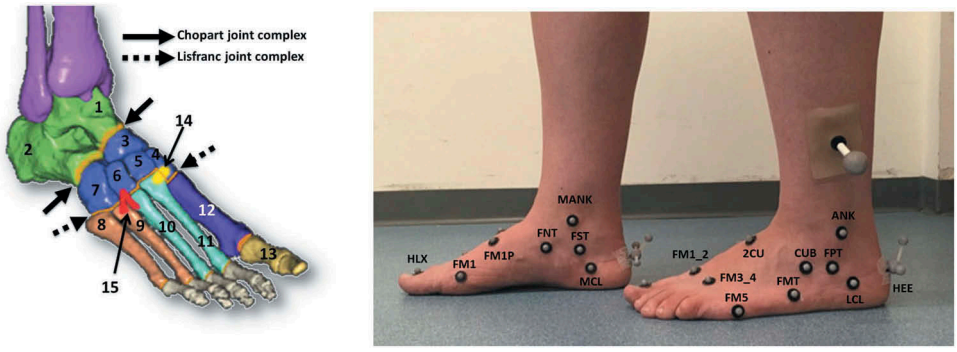

Figure 1. Multisegment foot model (left) and marker set (right).

Hindfoot (green), midfoot (blue), lateral forefoot (orange), central forefoot (turquoise), medial forefoot (indigo). Supplementary segments were shank (purple) and first toe (yellow). Chopart joint complex runs between talus (1) and calcaneus (2), and navicular (3) and cuboid (7). Lisfranc joint complex has three separate joint compartments: medial (between medial cuneiform (4) and metatarsal I (12)), central (linking intermediate (5) and lateral (6) cuneiforms to metatarsals II (11) and III (10), respectively), and lateral (between cuboid (7) and metatarsals IV (9) and V (10)). Lisfranc ligament (14) extends from the lateral surface of medial cuneiform (4) to the medial aspect of the base of metatarsal II (11). Lateral interosseous ligament (15) extends from the lateral surface of the lateral cuneiform (6) and ends on the lateral aspect of the base of metatarsal III (10) and sometimes on the medial aspect of the base of metatarsal IV (9).

2. Materials and methods

2.1. Participants

This study was approved by the Erasme-ULB ethical committee (approval number: B406201525145). Thirty adults (17 males and 13 females; mean age, 25 years (range, 18–38 years); and mean body mass index, 23.5 kg/m^2) with no history of musculoskeletal disorders were recruited. All subjects provided a written informed consent.

2.2. Multisegment foot model

The hindfoot (including talus and calcaneus (Carson et al. 2001)) and midfoot (including navicular, three cuneiforms, and cuboid (Leardini et al. 2007)) were defined according to previous publications. The forefoot division in this study was novel and included the following three compartments: lateral forefoot (including metatarsals V and IV), central forefoot (including metatarsals III and II), and medial forefoot (including metatarsal I).

2.2.1. Marker set

To define the foot model prior to gait analysis, 14 reflective markers (ϕ: 6 mm) were glued on the skin (Figure 1). All markers were placed on anatomical landmarks following a rigorous anatomic palpation procedure (Table 1) to guarantee better reproducibility (Van Sint Jan and Della Croce 2005; Van Sint Jan 2007).

Virtual landmarks (IS, IH, IM, and TOE) were used and obtained by identifying the midpoint between two reflective markers (Table 1). Furthermore, one supplementary cluster of four reflective markers (ϕ: 11 mm) was set on the hindfoot. Plug-in-Gait model was for marker placement of both the pelvis and thighs. For the shank (including tibia and fibula), four markers were placed, and a wand was set on the lateral aspect of each shank (Figure 1) (Leardini et al. 2007).

2.2.2. Anatomical reference frames

Anatomical frames were constructed from anatomical landmarks for each segment (Table 2 and Figure 2). Hindfoot and midfoot anatomical frames were created following the definition by Leardini (Leardini et al. 2007). Anatomical frame orientation was defined based on previous conventions (Wu and Cavanagh 1995): X-axis pointing forward, Y-axis pointing upward, and Z-axis pointing to the right for both sides.

2.2.3. Joint angles and foot architecture

Joint motion representation included three rotational degrees of freedom: dorsiflexion+/plantarflexion- (DP) around the Z-axis; inversion+/eversion- (IE) around the X-axis; and adduction+/abduction- (AA) around the Y-axis. Joint rotations were computed using a ZXY Euler angle sequence, which is equivalent to the Grood and Suntay sequence (Grood and Suntay 1983). No offset was applied.

Foot architecture was estimated using three additional measurements linked to foot deformation: **medial longitudinal arch angle** (the angle between the projection of the line segment FM1-FNT and that of FNT-MCL into the sagittal plane of the foot), **metatarsal arch height** (the distance between TOE and its projection perpendicular to a plane connecting FM1, FM5, MCL, and LCL), and **metatarsal arch width** (the distance between FM1 and FM5). The two latter were used to characterize metatarsal arch deformation. Measurements obtained during the static trial were used for normalizing distance parameters.

Table 1. Marker set.

Segments	Marker (M)/cluster (C) name	Anatomical or virtual landmarks	Palpation or building procedure
Shank	FNE (M)	Neck of fibula	Palpation book (Van Sint Jan 2007)
	TTC (M)	Tibial tuberosity	Palpation book (Van Sint Jan 2007)
	ANK (M)	Apex of lateral malleolus	Palpation book (Van Sint Jan 2007)
	MANK (M)	Apex of medial malleolus	Palpation book (Van Sint Jan 2007)
	IS	Virtual landmark	Midpoint between ANK and MANK
Hindfoot	HEE (C)	Posterior surface of calcaneus	Base marker set according to palpation book (Van Sint Jan 2007) + vertical marker along vertical axis of calcaneus
	FPT (M)	Peroneal trochlea	Palpation book (Van Sint Jan 2007)
	FST (M)	Sustentaculum tali	Palpation book (Van Sint Jan 2007)
	MCL (M)	Medial process of calcaneal tuberosity	Glide backward on the medial edge of the foot up to the medial process
	LCL (M)	Lateral process of calcaneal tuberosity	Glide backward on the lateral edge of the foot up to the lateral process
	IH	Virtual landmark	Midpoint between FPT and FST
Midfoot	2CU(M)	Intermediate cuneiform	To set the base marker, glide your finger backward on the dorsal surface of metatarsal II until reaching the joint between this bone and the intermediate cuneiform
	FNT (M)	Navicular tuberosity	Palpation book (Van Sint Jan 2007)
	CUB (M)	Cuboid	Behind FMT (see FMT definition below), a depression of soft tissues is palpated. Glide upward until you feel the most lateral point of the cuboid
	IM	Virtual landmark	Midpoint between CUB and FNT
Forefoot	FMT (M)	Tuberosity of metatarsal V	Glide backward on the lateral surface of metatarsal V until the most lateral point of the tuberosity
	FM5 (M)	Head of metatarsal V	Glide forward on the lateral surface of metatarsal V until the head; place the marker on center of the head
	FM3_4 (M)	Third interosseous space	Glide backward on the dorsal surface of the first phalanx of the fourth toe, cross the metatarsophalangeal TP joint, and place the marker medially between the heads of metatarsals III and IV
	FM1_2 (M)	First interosseous space	Glide backward on the dorsal surface of the first phalanx of the second toe, cross the metatarsophalangeal joint, and place the marker medially between the heads of metatarsals I and II
	FM1 (M)	Head of metatarsal I	Glide forward on the medial surface of metatarsal I until the head; place the marker on center of the head
	FM1P (M)	Base of metatarsal I	Glide backward on the medial surface of metatarsal I until the base (feel joint space and come back), glide upward to the extensor hallucis longus tendon, and place the marker medially to the tendon
	TOE	Virtual landmark	Midpoint between FM3_4 and FM1_2
Hallux	HLX (M)	Base of second phalanx of hallux	Just behind the toenail

Table 2. Anatomical frames building.

Shank:	**Lateral forefoot**:
•**O**: at IS	•**O**: at FMT
•**X**: perpendicular (⊥) to the plane containing MANK, ANK, and FNE	•**X**: from FMT to FM5
•**Z**: ⊥ to the plane defined by X and the line between IS and TTC	•**Y**: ⊥ to the plane defined by X and the line between FM3_4 and FM5
•**Y**: ⊥ to the plane defined by XZ	•**Z**: ⊥ to the plane defined by XY
Hindfoot:	**Central forefoot**:
•**O**: at HEE base	•**O**: at 2CU
•**X**: from HEE base to IH	•**X**: from 2CU to TOE
•**Z**: in the transversal plane defined by X and FST	•**Y**: ⊥ to the plane defined by X and the line between FM1_2 and FM3_4
•**Y**: ⊥ to the plane defined by XZ	•**Z**: ⊥ to the plane defined by XY
Midfoot:	**Medial forefoot**:
•**O**: at IM	•**O**: at FM1P
•**X**: from IM to 2CU	•**X**: from FM1P to FM1
•**Z**: in the transverse plane defined by X and FNT	•**Y**: ⊥ to the plane defined by X and the line between FM1 and FM1_2
•**Y**: ⊥ to the plane defined by XZ	•**Z**: ⊥ to the plane defined by XY

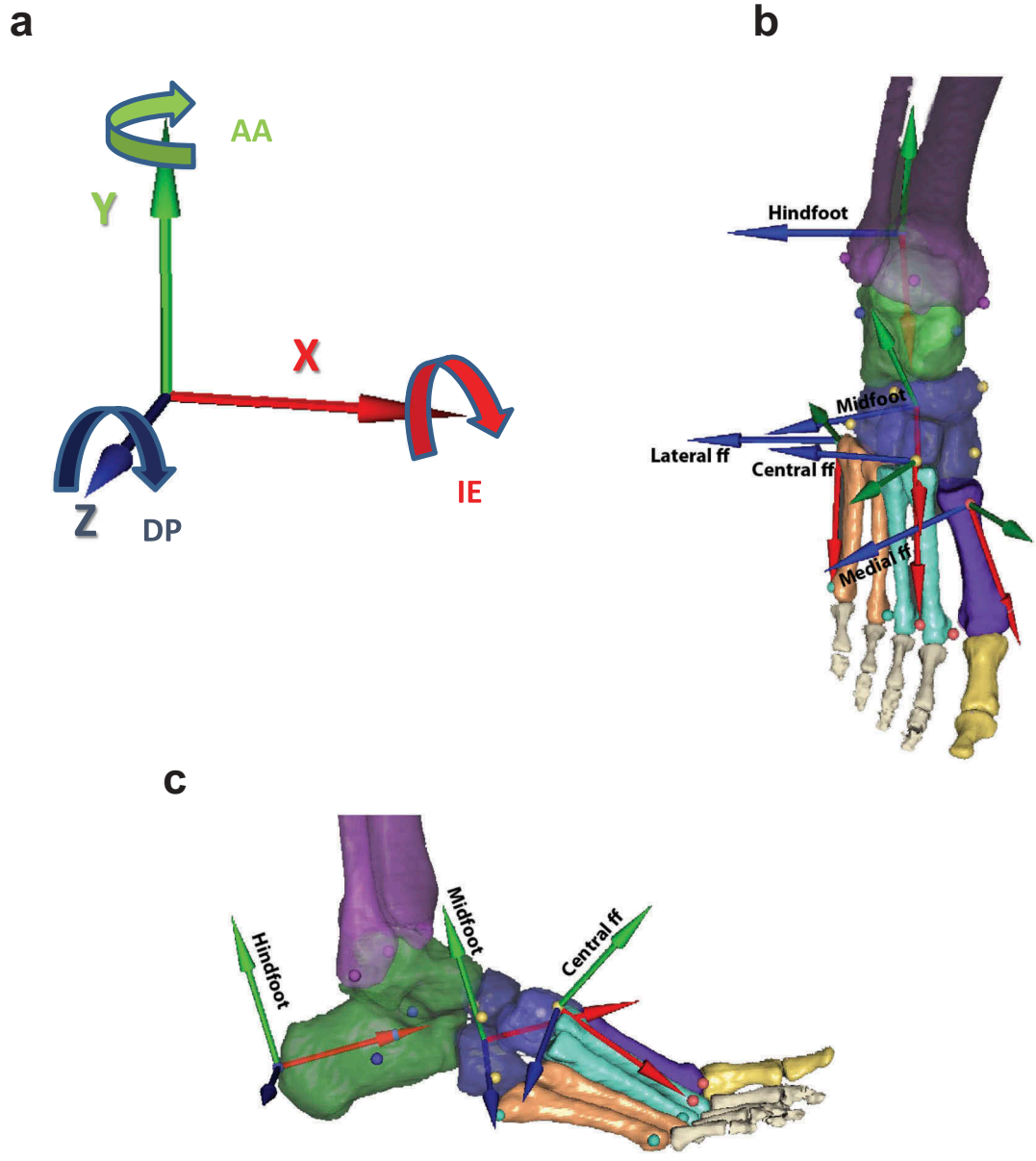

Figure 2. **Illustration of the obtained AFs.** (a). AF orientation: X-axis (red) is pointing forwards, Y-axis (green) is pointing upwards and Z-axis (blue) is pointing to the right (b). antero-superior view (ff = forefoot) (c). lateral view (ff = forefoot).

Note that AF construction leads to AFs that are oriented as much as possible according the segment-of-interest.

2.3. Data acquisition and analysis

Marker trajectories were recorded using an optoelectronic system (VICON T40s, 8 cameras, 100 Hz). Marker was labeled with the associated software (Nexus 1.7–1 Vicon Motion System, UK). For each subject, one static trial and five walking trials at a self-selected speed were recorded. Both left and right stance phases of all trials were analyzed and averaged. Joint angles between adjacent segments were computed from anatomical frame trajectories and expressed in the proximal segment (i.e. hindfoot relative to shank (HF/S), midfoot relative to hindfoot (MF/HF), lateral forefoot relative to midfoot (LFF/MF), central forefoot relative to midfoot (CFF/MF), and medial forefoot relative to midfoot (MFF/MF)). For data normalization, the curves were normalized to 100 time stamps using time events obtained from the ground reaction force (i.e. heel strike and toe off).

2.4. Forefoot model reliability

Repeatability and reproducibility assessment was performed by four raters, who are trained physical therapists, on six subjects during two sessions (1 h apart). For each session, a static trial (i.e. upright position) and five gait trials at a self-selected speed were performed. Between sessions, all foot markers but the cluster were removed.

Root mean square error was calculated for palpation precision. Joint angle variability was estimated for inter-trial, inter-session, and inter-rater conditions (Schwartz et al. 2004). Inter-trial deviations measured the stride-to-stride variability of gait pattern of each subject. For the inter-session variability of each rater, all first session trials were compared to all second session trials. For the inter-rater comparison, all trials of the four raters were compared. For the measurement of errors, the experimental error was estimated as the ratio between the inter-rater and inter-trial errors (Schwartz et al. 2004).

3. Results

3.1. Forefoot model reliability

For the palpation precision (Table 3), inter-rater variability (5.0 mm; SD, 0.8 mm) was higher than inter-session variability (2.0 mm; SD, 0.5 mm). Marker placement on the first metatarsal bone (FM1P and FM1) was the most variable.

For the error propagation on kinematic curves of the forefoot (Table 4), for each rotation, inter-rater variability was greater than inter-session variability, which was greater than inter-trial variability. Inter-trial errors ranged from 0.6° to 2.0°. Inter-session errors ranged from 1.4° to 3.2°. Inter-rater errors ranged from 2.1° to 5.5°. The largest intrinsic errors were observed in AA of the lateral and central forefoot (2.0°). Among all the axes, the medial forefoot presented the largest errors for inter-trial (1.4°), inter-session (2.5°), and inter-rater (4.0°) measurements, and the lateral forefoot was the most influenced by experimental errors (3.5). All segments combined, AA movement presented the largest errors for inter-trial (1.9°), inter-session (2.8°), and inter-rater (4.4°) measurements, and DP was the most influenced by experimental errors (3.3).

Table 3. Palpation precision of forefoot markers (mm, mean (SD)).

	FM1P	FM1	FM1_2	FM3_4	FM5	FMT
Inter-session	1.9 (0.3)	2.4 (0.7)	2.0 (0.2)	1.8 (0.5)	1.9 (0.4)	1.9 (0.8)
Inter-rater	6.6 (1.6)	5.4 (0.4)	3.5 (0.7)	4.8 (1.0)	4.2 (0.7)	5.2 (0.4)

3.2. Foot kinematics

3.2.1. Hindfoot

Initially, the HF/S plantarflexed, everted, and adducted at heel strike (Figure 3(a)). During loading response and midstance, dorsiflexion, eversion, and abduction were observed. Eventually, plantarflexion, inversion, and adduction occurred during the terminal stance and preswing phases. The DP, IE, and AA ranges of motion (RoM) were 20° (standard deviation (SD), 4°), 6° (SD, 2°), and 4° (SD, 2°), respectively. Peak dorsiflexion was observed at 67% (SD, 10%) of the stance phase.

3.2.2. Midfoot

Small RoM were observed for the midfoot (DP, 7° (SD, 2°); IE, 2° (SD, 1°); and AA, 4° (SD, 1°)). At the end of the stance phase, the MF/HF moved toward plantarflexion, inversion, and adduction (Figure 3(a)). Peak of dorsiflexion occurred at 73% (SD, 6%) of the stance phase.

3.2.3. Lateral forefoot

Initially, the LFF/MF showed plantarflexion at heel strike, which rapidly shifted toward dorsiflexion, eversion, and abduction during loading response (Figure 3(a)). Further, during the terminal stance and preswing phases, plantarflexion, inversion, and adduction were the main displacements. The DP, IE, and AA RoM were 6° (SD, 2°), 9° (SD, 3°), and 7° (SD, 2°), respectively. Peak inversion was observed at 88% (SD, 5%) of the stance phase; peak dorsiflexion, at 71% (SD, 8%) of the stance phase.

3.2.4. Medial forefoot

The MFF/MF plantarflexed at heel strike (Figure 3(a)). During loading response, dorsiflexion, eversion, and adduction were noted. Subsequently, during the terminal stance and preswing phases, plantarflexion, eversion, and

Table 4. Inter-trial, inter-session and inter-rater errors and experimental errors (mean (SD)).

		Inter-trial errors (°)	Inter-session errors (°)	Inter-rater errors (°)	Experimental errors
Lateral forefoot	DP	0.6 (0.1)	1.5 (0.1)	2.4 (0.1)	4.0
/midfoot	IE	0.7 (0.2)	1.5 (0.2)	2.6 (0.2)	3.7
	AA	2.0 (0.6)	3.2 (0.4)	5.5 (0.2)	2.8
	Mean	**1.1**	**2.1**	**3.5**	**3.5**
Medial forefoot	DP	1.2 (0.3)	2.2 (0.3)	3.6 (0.3)	2.9
/midfoot	IE	1.4 (0.7)	2.5 (0.6)	4.1 (0.7)	2.9
	AA	1.6 (0.6)	2.7 (0.6)	4.4 (0.4)	2.8
	Mean	**1.4**	**2.5**	**4.0**	**2.9**
Central forefoot	DP	0.9 (0.2)	1.7 (0.1)	2.8 (0.2)	2.9
/midfoot	IE	1.0 (0.4)	1.4 (0.4)	2.1 (0.5)	2.1
	AA	2.0 (0.7)	2.4 (0.8)	3.2 (0.8)	1.6
	Mean	**1.3**	**1.8**	**2.7**	**2.2**

abduction were observed. The DP, IE, and AA RoM were 9° (SD, 4°), 7° (SD, 3°), and 3° (SD, 2°), respectively. Peak eversion was observed at 85% (SD, 8%) of the stance phase; peak dorsiflexion, at 70% (SD, 11%) of the stance phase.

3.2.5. Central forefoot

Initially, the CFF/MF plantarflexed at heel strike (Figure 3(a)). During loading response, dorsiflexion, eversion, and adduction were noted, and plantarflexion, inversion, and adduction were observed during the terminal stance and preswing phases. The DP, IE, and AA RoM were 9° (SD, 3°), 6° (SD, 2°), and 5° (SD, 2°), respectively. Peak dorsiflexion was observed at 72% (SD, 6%) of the stance phase.

3.3. Foot architecture

3.3.1. Medial longitudinal arch angle

During the whole stance, the medial longitudinal arch angle varied between 126° and 163°. From heel strike, this angle increased progressively to 146° (SD, 12°), which was obtained at 70% (SD, 6 %) of the stance phase (Figure 3(b)). Subsequently, the angle decreased rapidly until a minimum of 131°, which was observed at toe-off. In static acquisition, the mean of the medial longitudinal arch angle was 145° (SD, 8°) and varied between 127° and 162°.

3.3.2. Metatarsal arch height

In bipodal static position, the mean of the metatarsal arch height was 14 mm (SD, 3 mm) and varied between 8 mm and 22 mm. In gait, the metatarsal arch height increased progressively during mid-stance and rapidly during the terminal stance, with a peak (1.32) at 87% (SD, 4 %) of the stance phase (Figure 3(b)). For the entire stance phase, the arch height varied between 0.87 and 1.32 of the static measurement.

3.3.3. Metatarsal arch width

During gait, for the metatarsal arch width, a plateau of maxima (0.99 of the static value) was observed between 21 and 71% of the stance phase (Figure 3(b)). In static acquisition, the mean of the metatarsal arch width was 104 mm (SD, 8 mm) and varied between 92 mm and 130 mm.

4. Discussion

This study analyzed forefoot kinematics using a novel model based on three independent segments. The model was designed to quantify and assess forefoot arch-shaped architecture during gait. Results of this study showed that normal forefoot deformation is characterized by a measurable pattern during the stance phase of gait. Moreover, during loading response, the lateral forefoot quickly everted and abducted, while the medial forefoot everted and adducted gradually throughout the entire stance phase. Throughout the mid-stance phase, most of the kinematic curves showed a plateau, indicating no kinematic change in the forefoot. At terminal stance, the lateral forefoot inverted and adducted, while the medial forefoot everted and abducted to restore the metatarsal arch (Figure 4). Interestingly, metatarsal arch height, lateral forefoot inversion, and medial forefoot eversion reached their peak simultaneously at around 87% of the stance phase. The forefoot motions and metatarsal arch-shape observed in this study are consistent with the findings of a previous study (Duerinck et al. 2014), which is related to forefoot deformation and latero-medial forefoot rollover during stance phase. The medial longitudinal arch tended to flatten from the initial contact to the first part of terminal stance. Subsequently, all segments plantarflexed and medial longitudinal arch restoration occurred. The same curve was reported in a previous study (Simon et al. 2006). The largest arch angle (i.e. the most flattened arch) was noted at around 70% (SD, 6%) of the stance phase, and simultaneously, the peak of dorsiflexion of all five foot segments was observed. The peak of the drop of the navicular

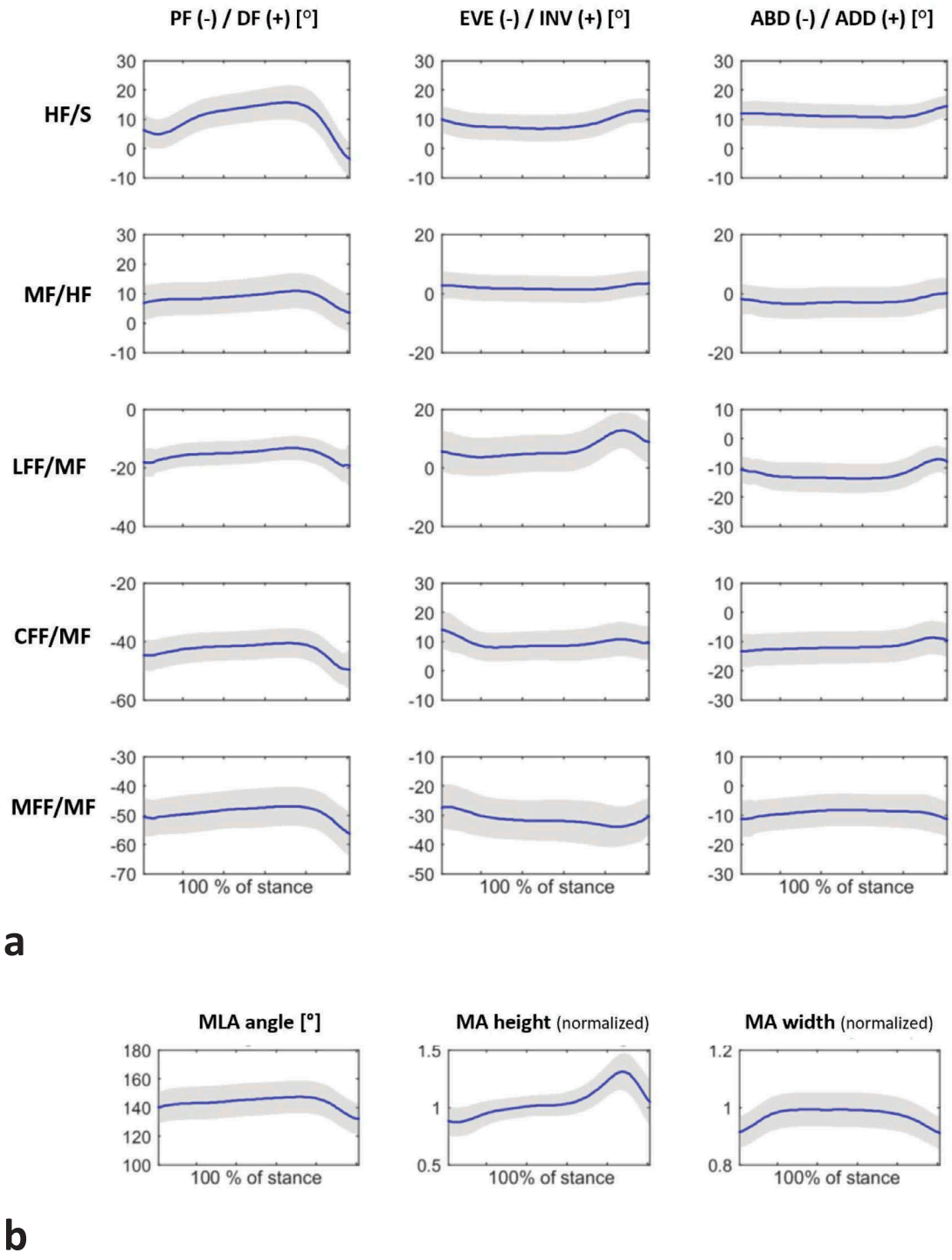

Figure 3. **Foot kinematics and arch-shaped curves during stance phase. (**a). Mean (blue line) and SD (grey) of joint rotation (°) for each segment of foot model as a function of percentage of stance phase for all 30 subjects over five repetitions. (b). Mean (blue line) and SD (grey) of changes in medial longitudinal arch (MLA) angle and metatarsal arch (MA) height and width as a function of percentage of stance phase for all 30 subjects over five repetitions.

tuberosity appeared around the same time (i.e. 73 to 77% of the stance phase), which corresponded to the second peak in the gait ground reaction force (Dicharry et al. 2009).

Lack of anatomical frames, offsets, and joint angle parameter standardization does not allow for a reliable comparison of kinematic curves with previous reports (Carson et al. 2001). However, our results concerning both the curve shape (i.e. movement direction) and RoM are in agreement with those of previous studies for both hindfoot (Carson et al. 2001; MacWilliams et al.

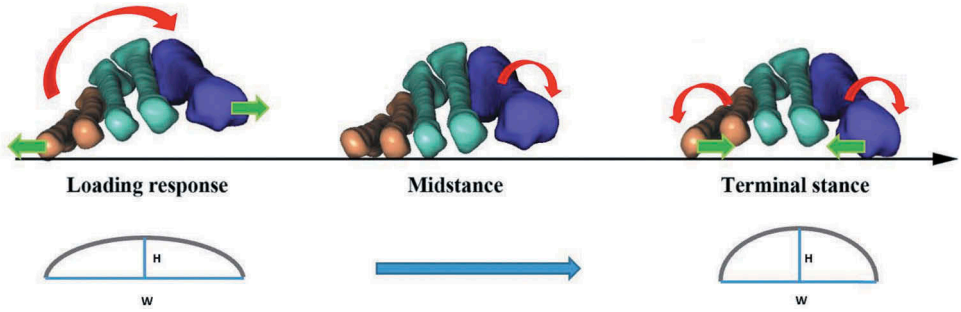

Figure 4. Forefoot motion and metatarsal arch deformation during the stance phase.

IE motion (red arrow) and AA motion (green arrow) of the lateral forefoot (orange), central forefoot (turquoise), and medial forefoot (indigo), and metatarsal arch deformation (height (H) and width (W))

2003; Leardini et al. 2007; Rankine et al. 2008) and midfoot (MacWilliams et al. 2003; Leardini et al. 2007; Rankine et al. 2008) (Figure 3(a)). Moreover, some of our observations of forefoot motion are similar to those of a previous study (MacWilliams et al. 2003). Firstly, the medial and central forefeet exhibited more plantar flexion than the lateral forefoot in later stance. Secondly, in early stance, the lateral forefoot generally combines dorsiflexion, eversion, and abduction, while plantarflexion, inversion, and adduction appeared during later stance. However, in our study, the medial forefoot shifted to eversion over the entire stance phase and to abduction in the late stance phase, which differs from the results of Mac Williams et al. This difference could be explained by the fact that the medial forefoot of Mac Williams et al. included metatarsals I, II, and III. This emphasizes the need to analyze metatarsal I behavior independently. In addition, studies questioning the use of a rigid forefoot model support our observation (Okita et al. 2009).

In the present model, the least reliable movement was adduction-abduction, as previously demonstrated (Siegel et al. 1995; Stebbins et al. 2006). Moreover, significant skin artifact was reported for adduction-abduction movements of the forefoot before foot flat and during late stance (Okita et al. 2009). Considering these facts and the small RoM, the interpretation of our results concerning adduction-abduction movement must be taken with caution. The most variable segment was the medial forefoot, which could be because a high variability of marker placement on the first metatarsal exists. However, the segment most influenced by experimental errors was the lateral forefoot because of its lowest intrinsic variability. The inter-trial variability was similar to previous reliability studies (Sawacha et al. 2009; Caravaggi et al. 2011; Deschamps et al. 2012; Saraswat et al. 2012) which took into account a whole forefoot. For the inter-rater variability, Saraswat's (Saraswat et al. 2012) and Sawacha's (Sawacha et al. 2009) studies observed less than 6° for all rotations of the forefoot, as in the proposed forefoot model. In Di Marco' study (Di Marco et al. 2016), the maximum difference obtained at initial contact and toe-off for the forefoot segment expressed in midfoot ranged between 1° (SD, 1°) and 3° (SD, 2°). The comparison with these results must be taken with caution given the difference in experimental condition (treadmill walking), statistical analysis (maximum difference) and selected point of kinematic curve (events). The reliability studies of Caravaggi (Caravaggi et al. 2011) and Deschamps (Deschamps et al. 2012) using the Leardini model, found generally higher inter-rater variability for the forefoot compared to the proposed forefoot model, resulting in a higher experimental error, respectively 4.3 and 5.6. Thus, the forefoot subdivision into three compartments does not increase variability and experimental error.

Four aspects of the proposed anatomical forefoot model seem to be of interest for future clinical applications. First, while disorders of other foot joints are possible, well-described motion assessment protocols are mostly available for the hindfoot. The proposed anatomical forefoot model enables motion analysis of supplementary segments and could lead to a fine-tuned understanding of normal and pathological forefoot behavior. Secondly, kinematic interpretation apparently varies when we consider the forefoot as either a whole or composed of several segments (Figure 3). Thirdly, the authors chose not to apply an offset to kinematic curves to highlight individual differences and possible static foot deformities. This is an obvious advantage for clinical reporting. Moreover, foot posture varies from one subject to another. Applying an offset to force kinematic curves to start at zero removes this individual variability (Carson et al. 2001; Deschamps et al. 2012; Røislien et al. 2012). Lastly, the combination of foot arch shape and kinematics provides a more clinical representation of foot biomechanics during walking.

Furthermore, the benefit of our model in pathological conditions, such as hallux valgus, is undeniable. Hallux valgus deformity is complex, and understanding of this condition remains incomplete (Easley and Trnka 2007). The association between hallux valgus, first metatarsal eversion, and medial longitudinal arch collapse has been confirmed (Eustace et al. 1994). Radiographic evaluation of the metatarsal arch in hallux valgus showed a lower position of the first, second, and third metatarsal heads (Suzuki et al. 2004). Thus, demonstrating the loss of metatarsal arch function during the propulsion phase to understand the pathology and to identify treatment strategies, such as improving insole design, seems essential. Subsequently, assessment of foot arch shape and forefoot kinematics in patients with hallux valgus should be conducted.

This study showed that metatarsal arch shape could be assessed during gait using the proposed three-compartment forefoot model. The results improved our understanding of forefoot kinematics and the role played by the arch in foot deformation. The kinematics obtained with a three-compartment anatomical forefoot model corroborates arch deformation. Moreover, an additional normative forefoot-related database is provided, which is needed for further clinical investigations. During stance phase, the foot is first compliant, and as it stabilizes, restoration of arches occurs at the end of the stance to support the propulsion (MacWilliams et al. 2003; Duerinck et al. 2014). The results and methods of this study highlight the potential of the three-segment model for use in clinical decision-making.

Acknowledgments

The authors would like to thank Mr. H. Bajou, Mr. H. Huault, Mr. P. Martin-Sisteron, Mr. A. Rodero and Mr. JL. Sterckx for their technical assistance, Mr. A. Stenhouse and Mrs. D. Ayadi for their clinical interpretation, and Mr. T. Leloup and Mrs. C. Verhoeven for their scientific support.

Declarations of interest statement

The authors report no conflict of interest.

Disclosure statement

No potential conflict of interest was reported by the authors.

ORCID

Véronique Feipel http://orcid.org/0000-0002-0146-3731

References

Bojsen-Møoller F. 1979. Anatomy of the forefoot, normal and pathologic. Clin Orthop Relat Res. 142:10–18.

Caravaggi P, Benedetti MG, Berti L, Leardini A. 2011. Repeatability of a multi-segment foot protocol in adult subjects. Gait Posture. 33:133–135.

Carson MC, Harrington ME, Thompson N, O'Connor JJ, Theologis TN. 2001. Kinematic analysis of a multi-segment foot model for research and clinical applications: a repeatability analysis. J Biomech. 34:1299–1307.

Castro M, Melão L, Canella C, Weber M, Negrão P, Trudell D, Resnick D. 2010. Lisfranc joint ligamentous complex: MRI with anatomic correlation in cadavers. AJR Am J Roentgenol. 195:W447–455.

Daentzer D, Wülker N, Zimmermann U. 2003. Observations concerning the transverse metatarsal arch. Foot Ankle Surg. 3:15–20.

De Doncker E, Kowalski C. 1979. Cinésiologie et rééducation du pied. Paris: Masson. French.

Deschamps K, Staes F, Bruyninckx H, Busschots E, Matricali GA, Spaepen P, Meyer C, Desloovere K. 2012. Repeatability of a 3D multi-segment foot model protocol in presence of foot deformities. Gait Posture. 36:635–638.

Di Marco R, Rossi S, Racic V, Cappa P, Mazza C. 2016. Concurrent repeatability and reproducibility analyses of four marker placement for the foot-ankle complex. J Biomech. 49:3168–3176.

Dicharry JM, Franz JR, Della Croce U, Wilder RP, Riley PO, Kerrigan DC. 2009. Differences in static and dynamic measures in evaluation of talonavicular mobility in gait. J Orthop Sports Phys Ther. 39:628–634.

Duerinck S, Hagman F, Jonkers I, Van Roy P, Vaes P. 2014. Forefoot deformation during stance: does the forefoot collapse during loading? Gait Posture. 39:40–47.

Easley ME, Trnka H-J. 2007. Current concepts review: hallux Valgus Part 1: pathomechanics, clinical assessment, and nonoperative management. Foot Ankle Int. 28:654–659.

Eustace S, Byrne JO, Beausang O, Codd M, Stack J, Stephens MM. 1994. Hallux valgus, first metatarsal pronation and collapse of the medial longitudinal arch — a radiological correlation. Skeletal Radiol. 23:191–194.

Grampp J, Willson J, Kernozek T. 2000. The plantar loading variations to uphill and downhill gradients during treadmill walking. Foot Ankle Int. 21:227–231.

Grood ES, Suntay WJ. 1983. A joint coordinate system for the clinical description of three-dimensional motions: application to the knee. J Biomech Eng. 105:136–144.

Jenkyn TR, Nicol AC. 2007. A multi-segment kinematic model of the foot with a novel definition of forefoot motion for use in clinical gait analysis during walking. J Biomech. 40:3271–3278.

Kanatli U, Yetkin H, Bolukbasi S. 2003. Evaluation of the transverse metatarsal arch of the foot with gait analysis. Arch Orthop Trauma Surg. 123:148–150.

Kapandji AI. 2011. Physiology of the joints: The lower limb (vol.2). 6th ed. Edinburgh and New York: Churchill Livingstone/Elsevier. [accessed 2018 Jun 27] https://www.elsevier.com/books/physiology-of-the-joints/kapandji/978-0-7020-3942-3

Komenda GA, Myerson MS, Biddinger KR. 1996. Results of arthrodesis of the tarsometatarsal joints after traumatic injury. J Bone Joint Surg Am. 78:1665–1676.

Leardini A, Benedetti MG, Berti L, Bettinelli D, Nativo R, Giannini S. 2007. Rear-foot, mid-foot and fore-foot motion during the stance phase of gait. Gait Posture. 25:453–462.

Luger EJ, Nissan M, Karpf A, Steinberg EL, Dekel S. 1999. Patterns of weight distribution under the metatarsal heads. J Bone Joint Surg [Br]. [accessed 2018 Jun 20]. https://online.boneandjoint.org.uk/doi/pdf/10.1302/0301-620X.81B2.0810199

MacWilliams BA, Cowley M, Nicholson DE. 2003. Foot kinematics and kinetics during adolescent gait. Gait Posture. 17:214–224.

Nester CJ, Liu AM, Ward E, Howard D, Cocheba J, Derrick T, Patterson P. 2007. In vitro study of foot kinematics using a dynamic walking cadaver model. J Biomech. 40:1927–1937.

Okita N, Meyers SA, Challis JH, Sharkey NA. 2009. An objective evaluation of a segmented foot model. Gait Posture. 30:27–34.

Queen RM, Abbey AN, Wiegerinck JI, Yoder JC, Nunley JA. 2010. Effect of shoe type on plantar pressure: a gender comparison. Gait Posture. 31:18–22.

Rankine L, Long J, Canseco K, Harris G. 2008. Multisegmental foot modeling: a review. Crit Rev Biomed Eng. 36:127–181.

Røislien J, Skare Ø, Opheim A, Rennie L. 2012. Evaluating the properties of the coefficient of multiple correlation (CMC) for kinematic gait data. J Biomech. 45:2014–2018.

Rouhani H, Favre J, Crevoisier X, Jolles BM, Aminian K. 2011. Segmentation of foot and ankle complex based on kinematic criteria. Comput Methods Biomech Biomed Engin. 14:773–781.

Saraswat P, MacWilliams BA, Davis RB. 2012. A multi-segment foot model based on anatomically registered technical coordinate systems: method repeatability in pediatric feet. Gait Posture. 35:547–555.

Sawacha Z, Cristoferi G, Guarneri G, Corazza S, Donà G, Denti P, Facchinetti A, Avogaro A, Cobelli C. 2009. Characterizing multisegment foot kinematics during gait in diabetic foot patients. J Neuroeng Rehabil. 6:37.

Schwartz MH, Trost JP, Wervey RA. 2004. Measurement and management of errors in quantitative gait data. Gait Posture. 20:196–203.

Siegel KL, Kepple TM, O'Connell PG, Gerber LH, Stanhope SJ. 1995. A technique to evaluate foot function during the stance phase of gait. Foot Ankle Int. 16:764–770.

Simon J, Doederlein L, McIntosh AS, Metaxiotis D, Bock HG, Wolf SI. 2006. The Heidelberg foot measurement method: development, description and assessment. Gait Posture. 23:411–424.

Simonsen O, Vuust M, Understrup B, Højbjerre M, Bøttcher S, Voigt M. 2009. The transverse forefoot arch demonstrated by a novel X-ray projection. Foot Ankle Surg. 15:7–13.

Stebbins J, Harrington M, Thompson N, Zavatsky A, Theologis T. 2006. Repeatability of a model for measuring multi-segment foot kinematics in children. Gait Posture. 23:401–410.

Suzuki J, Tanaka Y, Takaoka T, Kadono K, Takakura Y. 2004. Axial radiographic evaluation in hallux valgus: evaluation of the transverse arch in the forefoot. J Orthop Sci. 9:446–451.

Tome J, Nawoczenski DA, Flemister A, Houck J. 2006. Comparison of foot kinematics between subjects with posterior tibialis tendon dysfunction and healthy controls. J Orthop Sports Phys Ther. 36:635–644.

Tschauner C, Kohlmaier W. 1997. Ultrasonographic evaluation of the transverse metatarsal arch. Foot Ankle Surg. 3:41–48.

van der Zwaard BC, Vanwanseele B, Holtkamp F, van der Horst HE, Elders PJ, Menz HB. 2014. Variation in the location of the shoe sole flexion point influences plantar loading patterns during gait. J Foot Ankle Res. 7:20.

Van Sint Jan S. 2007. Color atlas of skeletal landmark definitions: guidelines for reproducible manual and virtual palpations. Chapter 17: Tibia, p. 142–150. Chapter 18: Fibula, p. 152–159. Chapter 19: Foot; p. 160–175. London: Churchill Livingstone/Elsevier.

Van Sint Jan S, Della Croce U. 2005. Identifying the location of human skeletal landmarks: why standardized definitions are necessary-a proposal. Clin Biomech Bristol Avon. 20:659–660.

Wu G, Cavanagh PR. 1995. ISB recommendations for standardization in the reporting of kinematic data. J Biomech. 28:1257–1261.